Powder Technology 247 (2013) 60–68

Contents lists available at ScienceDirect

Powder Technology

journal homepage: www.elsevier.com/locate/powtec

# Process intensification of $BaSO_4$ nanoparticle preparation with agitation of microbubbles ☆

L. Du, Y.J. Wang, Y.C. Lu, G.S. Luo *

*The State Key Laboratory of Chemical Engineering, Department of Chemical Engineering, Tsinghua University, Beijing 100084, People's Republic of China*

ARTICLE INFO

*Article history:*
Received 26 January 2013
Received in revised form 17 June 2013
Accepted 23 June 2013
Available online 2 July 2013

*Keywords:*
$BaSO_4$ nanoparticles
Barite industry
Microbubbles
Mixing performance

ABSTRACT

This study presents a novel technique for the controllable preparation of $BaSO_4$ nanoparticles via the introduction of microbubbles into the reaction system. A high-concentration system based on barite industry was used, with saturated aqueous $Na_2SO_4$ and BaS solutions as the reactants. Microbubbles were generated by a membrane dispersion microreactor. The mixing performance was characterized using parallel competing reactions. The effects of various operation parameters on the nanoparticles were determined, and the reaction conditions were optimized. The results showed that the mixing performance could be improved by introducing microbubbles. The $BaSO_4$ nanoparticles were controllably prepared, with a relatively narrow size distribution. The average particle size could likewise be reduced to approximately 40 nm. A dimensionless micromixing scale of the microbubble flow was defined, and a model for predicting the $BaSO_4$ particle size was proposed. The calculated results were consistent with the experimental data.

© 2013 The Authors. Published by Elsevier B.V. All rights reserved.

## 1. Introduction

Barium sulfate ($BaSO_4$) is an important inorganic chemical that is primarily used in the filling materials and additives of plastics, paints, cosmetics, ceramics, pigments, and paper, among others [1,2]. Nano-sized $BaSO_4$ particles (<100 nm), in particular, exhibit outstanding properties that are primarily useful in high-class resin and rubber [3]. The traditional techniques for $BaSO_4$ industrial production include (1) precipitation between a saturated BaS aqueous solution (generated from the calcination of barite and coal) and a saturated $Na_2SO_4$ aqueous solution, (2) ball milling of the barite raw material, and (3) a reaction between aqueous solutions of $BaCO_3$ (generated from the high-temperature solid-phase synthesis of barite and $Na_2CO_3$) and $H_2SO_4$. The first of these routes is the most widely used in the industrial production of $BaSO_4$ nanoparticles, with $Na_2SO_4$ and BaS as the raw materials [4] (Fig. 1a). The reaction formula is shown as follows:

$$BaS + Na_2SO_4 \rightarrow BaSO_4 + Na_2S. \quad (1)$$

However, inefficient mixing and high reactant concentrations of the said reaction system make it very difficult to produce nanoparticles with a narrow particle size distribution. The technique requires high energy consumption, and the resulting $BaSO_4$ products are low-quality micro-sized particles (with a minimum size of approximately 1 μm) [5].

Microfluidics has become one of the best strategies for effective mixing during nanoparticle synthesis [6–8]. Microfluidic devices have several advantages with respect to nanoparticle preparation, such as their uniform flow and mixing conditions [9,10]. $BaSO_4$ nanoparticles have been successfully synthesized using microfluidic techniques [11]. However, these strategies usually employ $BaCl_2$ as the reactant, instead of the industrial raw material BaS. Furthermore, synthesis occurs at low concentrations and feed rates, which makes their scale-up from the laboratory to commercial production uneconomical [12]. On the other hand, theoretical models have been developed for $BaSO_4$ precipitation systems. Cheng et al. [13] utilized computational fluid dynamics (CFD) to simulate the nucleation and growth of $BaSO_4$ nanoparticles in a continuously stirred tank. Wei et al. [14], Rousseaux et al. [15], Baldyga et al. [16], and other investigators have reported similar results. Most of the models used population balance methods to predict the nucleation, growth, and agglomeration of nanoparticles [31]. The accuracy of the model has been objectively confirmed for predicting the nanoparticle sizes of $BaSO_4$, ZnO, and other organic materials [32,33]. However, models combining the mass transfer process and particle formation have not been analyzed to the same extent, particularly for precipitation under different mixing conditions.

The technology of $BaSO_4$ preparation using high concentrations of BaS and $Na_2SO_4$ is important in terms of atom economy because the $Na_2S$ product is an important chemical for dyeing and leather production; such a process sufficiently utilizes existing raw materials [17].

☆ This is an open-access article distributed under the terms of the Creative Commons Attribution-NonCommercial-ShareAlike License, which permits non-commercial use, distribution, and reproduction in any medium, provided the original author and source are credited.

* Corresponding author. Tel.: +86 1062783870; fax: +86 1062780304.
*E-mail address:* gsluo@tsinghua.edu.cn (G.S. Luo).

0032-5910/$ – see front matter © 2013 The Authors. Published by Elsevier B.V. All rights reserved.
http://dx.doi.org/10.1016/j.powtec.2013.06.030

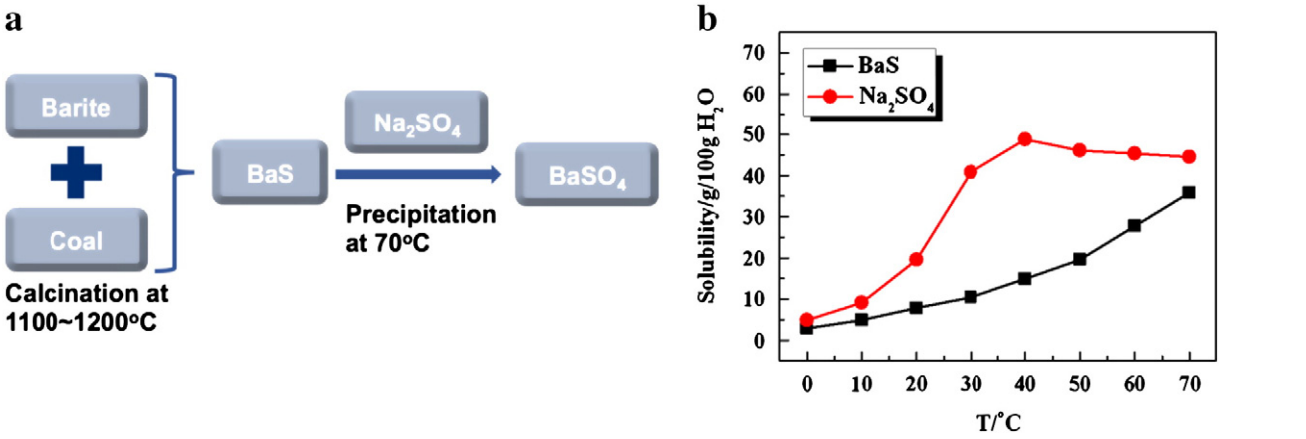


**Fig. 1.** (a) The industrial technique for producing $BaSO_4$ with BaS and $Na_2SO_4$; (b) the solubility of BaS and $Na_2SO_4$ in water under different temperatures.

Microfluidic techniques for efficient mixing based on advection induced by microbubbly flow interactions have attracted much attention [18,19]. Hydrodynamic interaction occurs in the gas–liquid flow, which increases the contact area for rapid mixing and homogenization [20,21]. No impurities are introduced in the mixing fluids, and the bubbles of the nitrogen/inert gas may be conveniently separated. In our previous study, a membrane dispersion microreactor was developed and successfully used to prepare nanoparticles in homogeneous and heterogeneous mixing systems [22–24]. The mixing scale of the liquid–liquid homogeneous flow and the process of nanoparticle preparation in the said membrane dispersion microreactor were modeled [25,26].

In this study, a novel method for the preparation of $BaSO_4$ nanoparticles has been developed using double membrane dispersion. The saturated BaS and $Na_2SO_4$ solutions were selected as the reactants for the preparation of $BaSO_4$ nanoparticles. Microbubbles of $N_2$ gas were introduced into the reaction system to enhance the mixing performance of the proposed method. The mixing performance was characterized using parallel competing reactions to explore the influence of the microbubbles. A dimensionless micromixing scale of the microbubbly flow was proposed and demonstrated.

## 2. Materials and experimental procedures

Based on the existing conditions of industrial production, saturated $Na_2SO_4$ and BaS solutions at different reaction temperatures were chosen as the raw materials. The solubility of these two reactants is temperature-sensitive, as shown in Fig. 1b. The solubility of BaS changes from 2.9 g to 35.8 g for every 100 g of water, whereas that of $Na_2SO_4$ changes from 4.9 g to 44.5 g for every 100 g of water. Thus, the concentration increases with the temperature, and the synthesis process requires effective mixing performance for the high-concentration system.

### 2.1. Preparation of $BaSO_4$ nanoparticles

The experimental set-up is shown in Fig. 2, where two membrane dispersion microdevices were used. Micro-filtration membranes (purchased from the Central Iron & Steel Research Institute, Beijing, PR China) were introduced to the systems; these membranes had an average pore size of 0.5 μm, an area of 12.5 $mm^2$, and a porosity of 65%. The geometric size of the main channel was 20 mm × 2 mm × 0.5 mm (length × width × height). $BaSO_4$ preparation was performed in two modes. Mode I involved the introduction of the $N_2$ gas (99.999%, 0.3 MPa) microbubbles; both Devices 1 and 2 were used. Mode II was performed without the gas microbubbles, and only Device 2 was employed.

In Mode I, the $Na_2SO_4$ solution (0.15 mol·$L^{-1}$ to 0.32 mol·$L^{-1}$) was first introduced as the continuous feed, which was mixed with the $N_2$ gas (0.3 MPa) in Device 1. The pressure difference between the two sides of the membrane was utilized as the driving force to disperse the $N_2$ gas as microbubbles in the continuous feed. The gas-mixed $Na_2SO_4$ solution was then mixed with the dispersed feed of the BaS solution (0.5 mol·$L^{-1}$ to 2.2 mol·$L^{-1}$) in Device 2. The $BaSO_4$ nanoparticles were synthesized when the two feeds interacted with each other in the mixing chamber. After aging treatment for 1 h, the $BaSO_4$ precipitates were separated from the suspension using a centrifugal separator (LD5-2A; Beijing Medical Centrifugal Separator Factory). The $BaSO_4$ precipitates were washed thrice with distilled water, twice with ethanol, and then incubated in a drying cabinet at 100 °C for 24 h to obtain the final $BaSO_4$ product.

The morphologies of the nanoparticles were recorded by transmission electron microscopy (TEM). A JEOL-2010 microscope with a high speed CCD video camera was used to record and measure the diameter of the microbubbles at magnifications of 20× to 200×. The crystal form of the nanoparticles was characterized by X-ray diffraction analysis (XRD; Rigaku Corporation D/max-RB).

### 2.2. Mixing performance

The "Villermaux/Dushman method" was utilized to characterize the mixing performance in the preparation process, with or without the

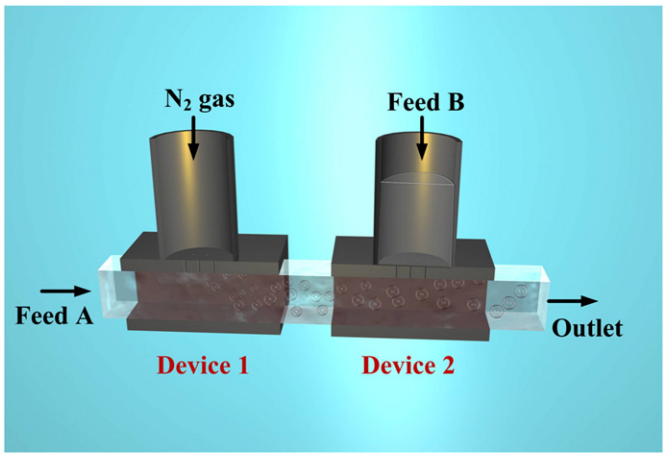


**Fig. 2.** The experimental set-up. (1) Preparation of $BaSO_4$ nanoparticles, Feed A: saturated $Na_2SO_4$ solution, Feed B: saturated BaS solution; (2) characterization of the mixing performance, Feed A: the solution containing KI, $KIO_3$, $NaH_2BO_3$ and $H_3BO_3$, Feed B: diluted sulfuric acid solution.

introduction of microbubbles [27]. The following reaction formulas were involved:

$$H_2BO_3^- + H^+ \rightarrow H_3BO_3 \quad \text{(quasi-instantaneous)} \tag{2}$$

$$5I^- + IO_3^- + 6H^+ \rightarrow 3I_2 + 3H_2O \quad \text{(fast)} \tag{3}$$

$$I_2 + I^- \leftrightarrow I_3^-. \tag{4}$$

The absorbance of the product triiodide was measured by spectrophotometry (UV–vis recording spectrophotometer, UV-8345; Hewlett–Packard) at 353 and 286 nm. The segregation index $X_S$ was defined based on the absorbance values, as

$$X_S = \frac{Y}{Y_{ST}} = \frac{\left(C_{I_2} + C_{I_3^-}\right)V}{n_{H^+,0}} \left(\frac{6C_{IO_3^-,0} + C_{H_2BO_3^-,0}}{3C_{IO_3^-,0}}\right) \tag{5}$$

where $n$ and $C$ are the number of moles and molar concentration of the subscript species, respectively; the subscript "0" represented their initial state. $Y$ is the ratio of the number of moles of the acid consumed in the reaction (Eq. (2)) to the total number of moles of the acid. $Y_{ST}$ is the value of $Y$ when the mixing process is infinitely slow. The value of $X_S$ lies between 0 and 1, which decreases with the improvement of

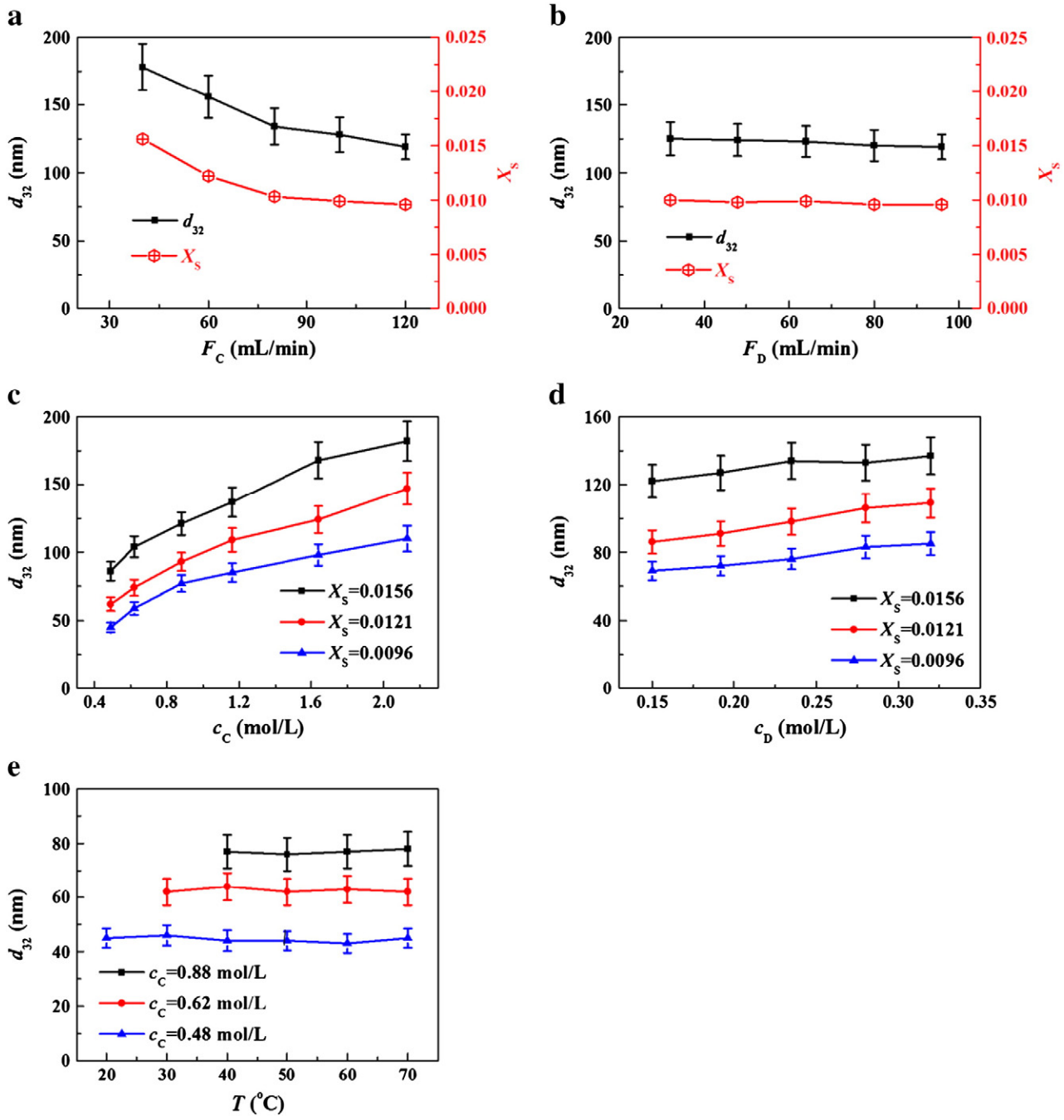


**Fig. 3.** Effects of feed flow rates, concentrations, and temperature on the segregation index and size of $BaSO_4$ nanoparticles: (a) BaS 2.12 mol·L$^{-1}$, $Na_2SO_4$ 0.32 mol·L$^{-1}$, $F_D$ = 64 mL·min$^{-1}$; (b) BaS 2.12 mol·L$^{-1}$, $Na_2SO_4$ 0.32 mol·L$^{-1}$, $F_C$ = 120 mL·min$^{-1}$; (c) $Na_2SO_4$ 0.32 mol·L$^{-1}$, $F_D$ = 48 mL·min$^{-1}$; (d) BaS 0.88 mol·L$^{-1}$, $F_D$ = 48 mol·L$^{-1}$; (e) $Na_2SO_4$ 0.18 mol·L$^{-1}$, $F_C$ = 120 mL·min$^{-1}$, $F_D$ = 64 mL·min$^{-1}$.

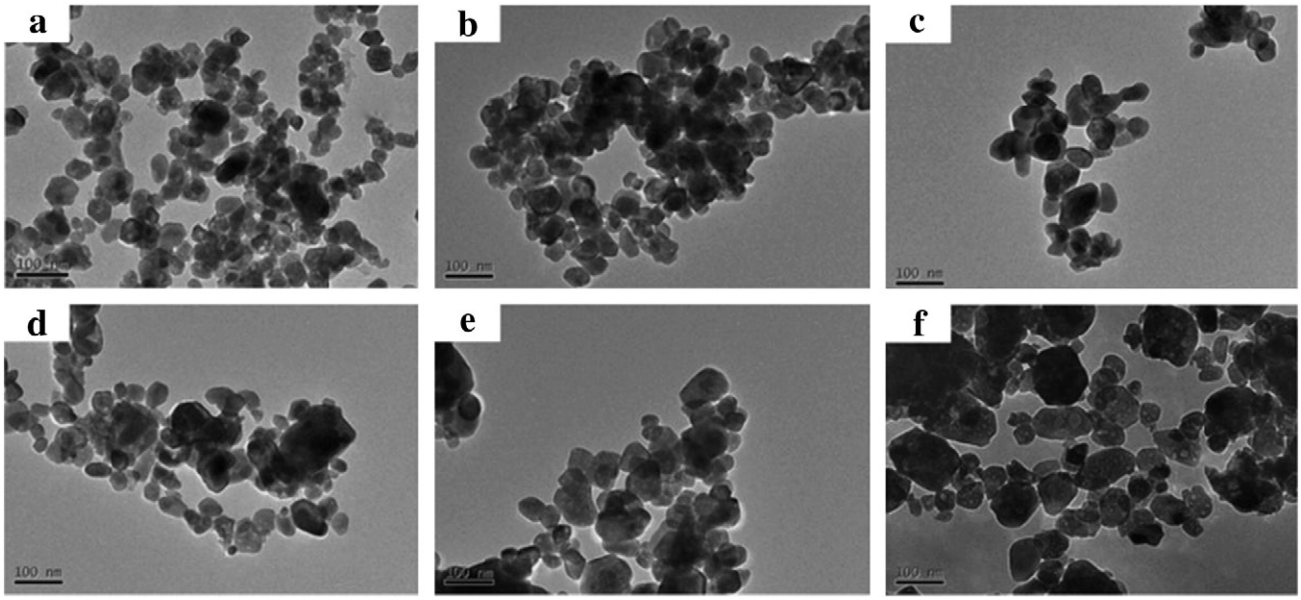


**Fig. 4.** TEM images of $BaSO_4$ nanoparticles synthesized at different concentrations. (a) BaS 0.48 mol·L$^{-1}$, $Na_2SO_4$ 0.16 mol·L$^{-1}$; (b) BaS 0.62 mol·L$^{-1}$, $Na_2SO_4$ 0.18 mol·L$^{-1}$; (c) BaS 0.88 mol·L$^{-1}$, $Na_2SO_4$ 0.22 mol·L$^{-1}$; (d) BaS 1.16 mol·L$^{-1}$, $Na_2SO_4$ 0.25 mol·L$^{-1}$; (e) BaS 1.64 mol·L$^{-1}$, $Na_2SO_4$ 0.30 mol·L$^{-1}$; (f) BaS 2.12 mol·L$^{-1}$, $Na_2SO_4$ 0.32 mol·L$^{-1}$.

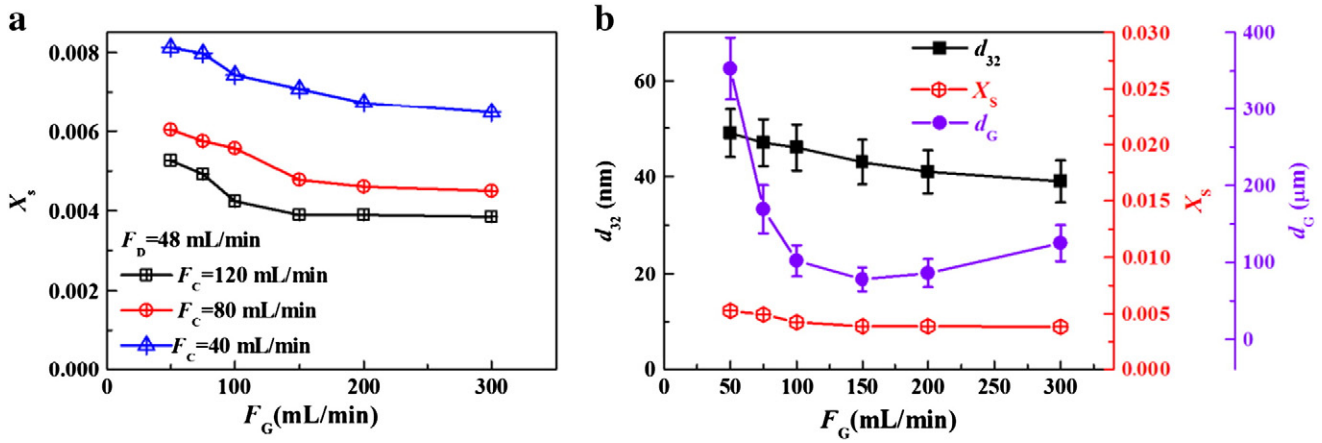


**Fig. 5.** (a) Effects of gas flow rate on $X_S$ at different continuous flow rates; (b) effects of gas flow rate on $d_G$, $d_{32}$ and $X_S$, BaS 2.12 mol·L$^{-1}$, $Na_2SO_4$ 0.32 mol·L$^{-1}$, $F_C$ = 120 mL·min$^{-1}$, $F_D$ = 48 mL·min$^{-1}$.

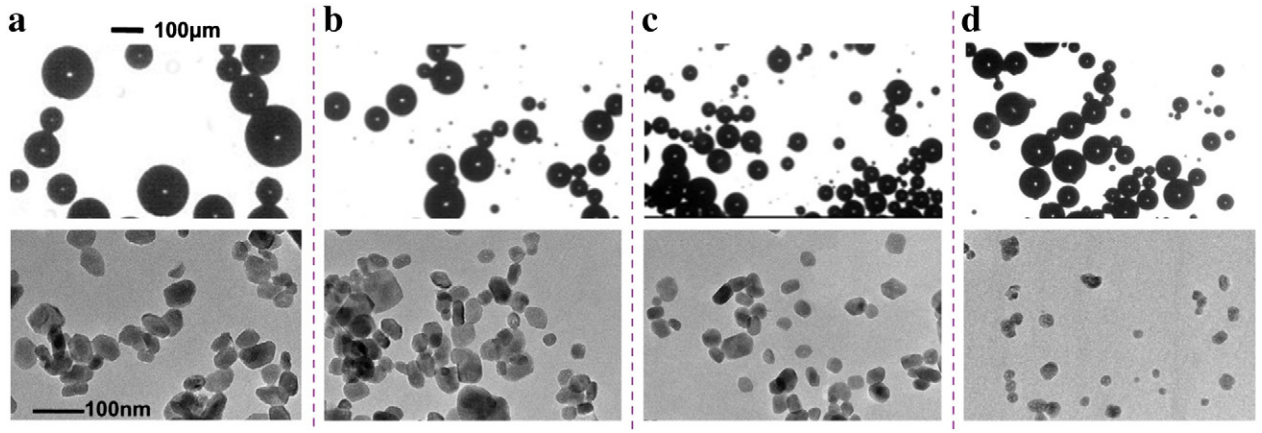


**Fig. 6.** Microscope images of microbubbles and TEM images of $BaSO_4$ nanoparticles. $F_C$ = 120 mL·min$^{-1}$, $F_D$ = 48 mL·min$^{-1}$, BaS 2.12 mol·L$^{-1}$, $Na_2SO_4$ 0.32 mol·L$^{-1}$: (a) $F_G$ = 50 mL·min$^{-1}$; (b) $F_G$ = 75 mL·min$^{-1}$; (c) $F_G$ = 150 mL·min$^{-1}$; (d) $F_G$ = 300 mL·min$^{-1}$.

mixing performance. $X_S = 0$ when there is perfect mixing; $X_S = 1$ in a completely segregated medium.

The mixing performance was mainly influenced by the operating conditions. Two reactant solutions were pumped into the microdevices, and the parallel competing reaction was then conducted to characterize the mixing performance. The competing reaction involved a dilute sulfuric acid solution as the dispersed solution in Feed B and a solution containing KI, $KIO_3$, $NaH_2BO_3$, and $H_3BO_3$ as the continuous solution in Feed A.

## 3. Results and discussion

### 3.1. Single-phase precipitation without microbubbles

The preparation was first performed without microbubbles using Device 2 alone. The influence of the operating conditions on the mixing performance and particle size was investigated.

The curves of $X_S$ varied with the flow rate in the microreactor (Fig. 3a and b). The $X_S$ and particle size decreased with the increasing

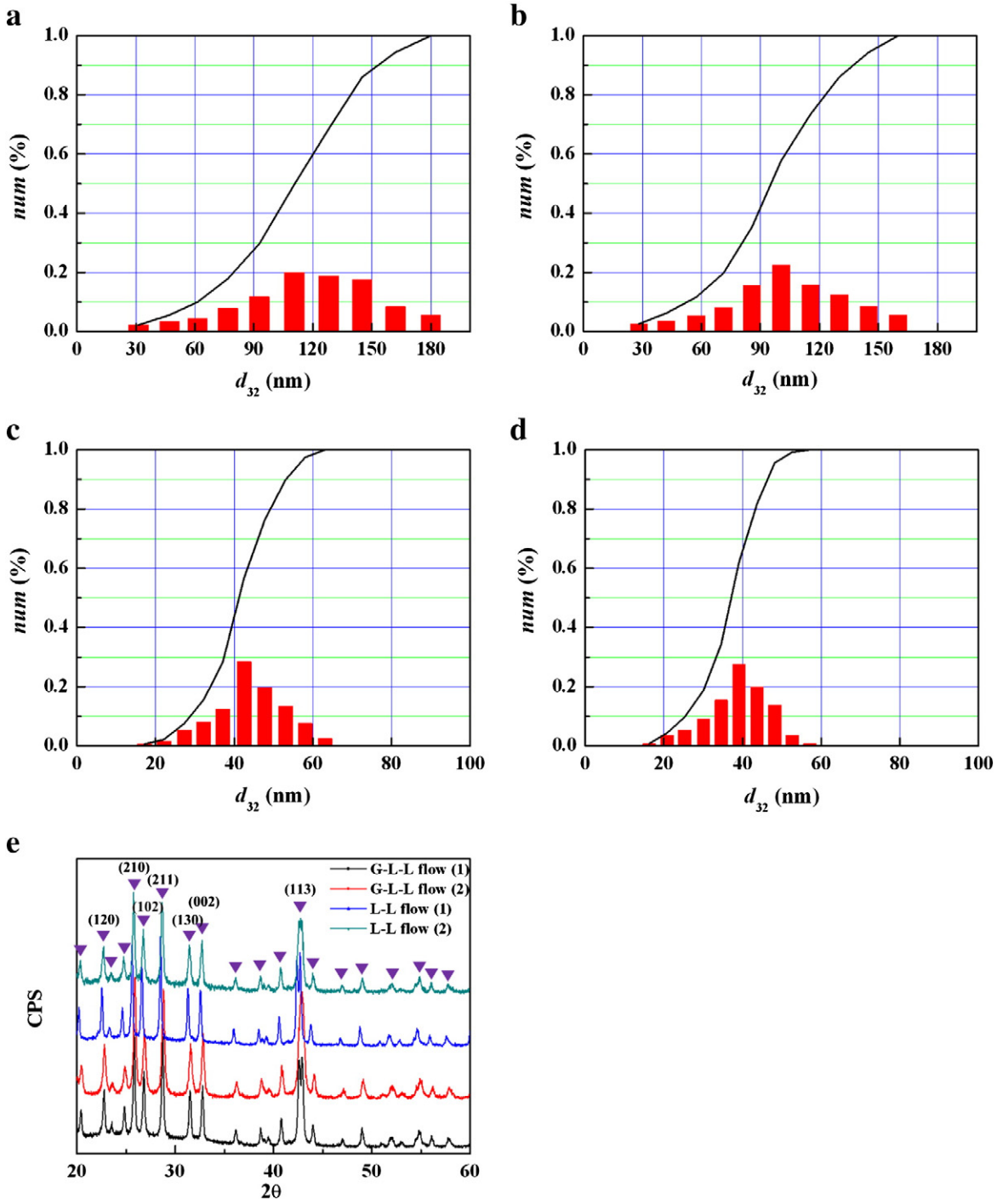


**Fig. 7.** (a–d) Particle size distributions of $BaSO_4$ nanoparticles: (a) BaS 2.12 mol·L$^{-1}$, $Na_2SO_4$ 0.32 mol·L$^{-1}$, $F_C$ = 100 mL·min$^{-1}$, $F_D$ = 50 mL·min$^{-1}$; (b) BaS 1.64 mol·L$^{-1}$, $Na_2SO_4$ 0.30 mol·L$^{-1}$, $F_C$ = 100 mL·min$^{-1}$, $F_D$ = 50 mL·min$^{-1}$; (c) BaS 2.12 mol·L$^{-1}$, $Na_2SO_4$ 0.32 mol·L$^{-1}$, $F_C$ = 40 mL·min$^{-1}$, $F_D$ = 25 mL·min$^{-1}$ $F_G$ = 60 mL·min$^{-1}$; (d) BaS 1.64 mol·L$^{-1}$, $Na_2SO_4$ 0.30 mol·L$^{-1}$, $F_C$ = 40 mL·min$^{-1}$, $F_D$ = 25 mL·min$^{-1}$ $F_G$ = 60 mL·min$^{-1}$; (e) XRD patterns of $BaSO_4$ powders: L–L flow (1), L–L flow (2), G–L–L flow (1), and G–L–L flow (2) correspond to the conditions in panels a to d, respectively.

flow rate of the continuous solution, as shown in Fig. 3a. The increased continuous feed flow rate provides a strong cross-flow shearing force, which reduces the mixing scale and shortens the mass transfer distance [28]. However, $X_S$ will not continue to decrease with the increased continuous flow rate unless there is efficient mixing. The $BaSO_4$ particle size still ranged from 110 nm to 200 nm. However, the $X_S$ and particle size did not significantly change with the flow rate of the dispersed solution (Fig. 3b). The disturbance of the mixture was enhanced and the mass transfer was strengthened when the flow rate of the dispersed solution was increased. However, the particle size of dispersed phase was simultaneously increased, which may decrease the mass transfer rate.

The particles were prepared in a wide range of reactant concentrations, as shown in Fig. 3c and d. The concentration of the BaS solution significantly influenced the particle size (Fig. 3c). However, the inefficient mixing at the concentration of 2.12 $mol \cdot L^{-1}$ caused an incomplete reaction, and the particles continued to grow after mixing. By contrast, the $Na_2SO_4$ solution did not greatly influence the particle size within the relatively smaller range (Fig. 3d). Precipitation was performed with the saturated BaS solutions of 20, 30, and 40 °C under different temperatures, as shown in Fig. 3e. The particle size was not affected by the reaction temperature because of the rapid precipitation of nanoparticles.

The TEM images of the $BaSO_4$ particles synthesized at different concentrations (Fig. 4) indicate that the nano-sized $BaSO_4$ particles can be prepared with single phase precipitation in the membrane dispersion microdevice. When the reactant concentration was increased, more particles with large sizes were generated, agglomeration simultaneously occurred, and the particle sizes became uneven. In other words, the particle size was synchronously increased with the supersaturation of $BaSO_4$, which played a leading role for the particles generated from precipitation [2,3,26]. The quality of the nanoparticles was significantly affected by the mixing performance, especially for the high-concentration systems based on industrial conditions. Thus, increasing the production capacity of the unit equipment can reduce the energy consumption and the amount of water. However, the mixing performance during synthesis still needs to be improved.

### 3.2. Preparation of $BaSO_4$ nanoparticles with the introduction of microbubbles

The introduction of microbubbles was hypothesized to increase the micromixing performance. Thus, two devices were used to investigate the influence of microbubbles on the mixing performance and particle size.

The curves of $X_S$ varied with the flow rates, as shown in Fig. 5a. $X_S$ was greatly reduced after the microbubbles were introduced to the system. The $X_S$ of the heterogeneous system (gas–liquid–liquid) was reduced by 30% to 80%, as compared with that of the homogeneous system (liquid–liquid). $X_S$ was one to two orders of magnitude smaller with the presence of microbubbles, as compared with the traditional mixing process [29]. Thus, the mixing performance was significantly improved by the introduction of microbubbles. Given the same total average flow rate, the $X_S$ of the heterogeneous system (Fig. 5a) was much smaller than that of the homogeneous system (Fig. 3b), thereby indicating the enhancing effect of the introduced microbubbles.

The effects of the gas flow rate on the microbubble and particle size are shown in Fig. 5b. Large microbubbles were generated at low gas flow rates, and the nanoparticle quality was improved. The increasing gas flow rate apparently reduced the bubble size; the smallest bubble diameter was reduced to approximately 40 nm to 60 nm. After the gas volume fraction was increased to 48%, the size of the bubbles started to increase, which may be attributed to bubble coalescence. $X_S$ was not increased despite the occurrence of coalescence, and the nanoparticle sizes were not increased. These results demonstrated that the particle size was primarily affected by the mixing efficiency, whereas the coalesced bubbles were important for turbulence and the secondary flow.

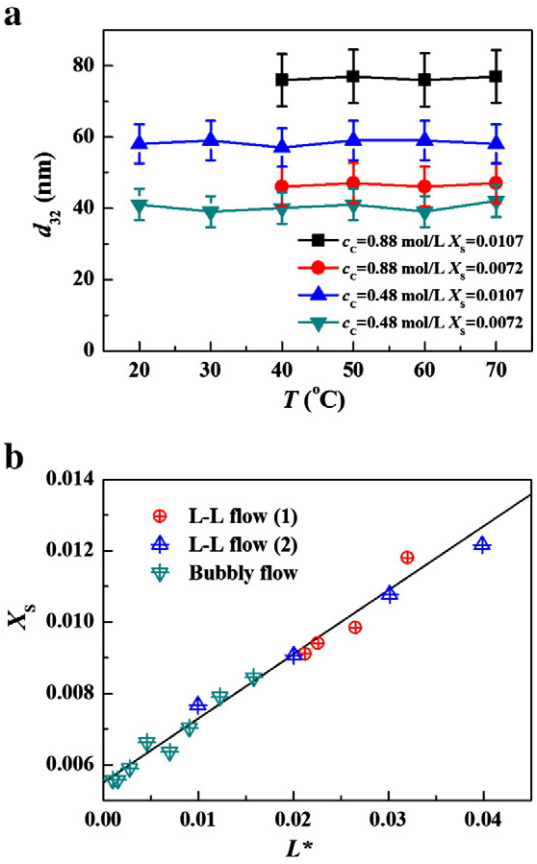


**Fig. 8.** (a) Effect of reaction temperature on the size of $BaSO_4$ nanoparticles at different concentrations and $X_S$; (b) segregation index varies with the dimensionless micromixing scale at different mixing conditions: L–L flow (1) represents 5 μm stainless steel membrane with $F_D$ of 16.3 $mL \cdot min^{-1}$, L–L flow (2) represents 5 μm stainless steel membrane with $F_C$ of 65.3 $mL \cdot min^{-1}$, [25] bubbly flow is according to $F_G$ of 200 $mL \cdot min^{-1}$, $F_C$ of 120 $mL \cdot min^{-1}$ and $F_D$ of 48 $mL \cdot min^{-1}$.

The micrographs of the microbubbles and the TEM images of nanoparticles at different gas flow rates are presented in Fig. 6. The introduction of the gas improved the monodispersity of the particles. The particles in the heterogeneous system were much smaller than those of the homogeneous precipitation at the same concentration. The particle size distributions from different heterogeneous reaction systems are shown in Fig. 7a to d. These results showed the narrow size distributions and smaller average sizes from the heterogeneous precipitation systems. The resulting XRD pattern is shown in Fig. 7e, which indicates that the $BaSO_4$ particles are crystals of an orthorhombic system and no characteristic peaks of BaS or $Na_2SO_4$ have been detected.

The influence of temperature on heterogeneous precipitation was likewise investigated, as shown in Fig. 8a. The particle size was not significantly affected by temperature for the same reactant concentrations

**Table 1**
Comparison with different strategies to synthesize $BaSO_4$ particles.

| Method | Reactants | Concentrations ($mol \cdot L^{-1}$) | Particle size (nm) |
|---|---|---|---|
| Industrial batch reactor [4] | BaS | 2.12 | 1000–2000 |
| | $Na_2SO_4$ | 0.32 | |
| Microreactor [12] | $BaCl_2$ | 0.1–1.0 | 12–40 |
| | $Na_2SO_4$ | 0.1 | |
| Microreactor [30] | $BaCl_2$ | 0.5 | 300–400 |
| | $Na_2SO_4$ | 0.1 | |
| Microbubbly flow (in this study) | BaS | 2.12 | 40–60 |
| | $Na_2SO_4$ | 0.32 | |

or levels of mixing efficiency. Given the rapid precipitation and continuous synthesis, the relatively short residence times had minimal effects on particle growth. The particle size was primarily influenced by the reactant concentration and mixing performance.

The preparation of the $BaSO_4$ nanoparticles with a microreactor was compared with other typical strategies, including the industrial technique [4,12,30]. The results of this comparison are summarized in Table 1. The dispersed microbubbly flow was excellent for both reactant categories and concentrations. The average particle sizes of the proposed system were comparable to those of other techniques that used $BaCl_2$ as the reactant. Furthermore, the concentration of the proposed method was 3 to 12 times higher than those of the other strategies. The proposed process could be continuously performed and controlled with relatively simple methods.

### 3.3. Modeling of the process with microbubbles

For the purpose of utilizing the classic precipitation model to describe the preparation of the proposed heterogeneous system, the process with microbubbles was modeled. Our previous work proposed a dimensionless micromixing scale ($L^*$) of the liquid–liquid phase, which is defined as follows [25]:

$$L^* = \frac{u_D}{u_T} = \frac{u_D}{u_D + u_C} \tag{6}$$

where $u_D$ and $u_C$ are the flow velocities of the dispersed and the continuous solutions, respectively. The relationship between the micromixing scale and $X_S$ was approximately linear, which could be described as

$$Xs = Xs_0 + K \cdot L* \tag{7}$$

The values of $K = 0.18$ and $Xs_0 = 0.0055$ were obtained for the membrane dispersion reactor. The influence of the gas flow rate, gas volume fraction, equivalent diameter, and bubble size upon the introduction of microbubbles were considered to modify the micromixing scale, which can be represented as

$$L^* = \frac{u_D}{u_T} \cdot \frac{S_{MR}}{S_{MR} + 4\pi R_G^2} \cdot \frac{\Phi V_{MR}}{\frac{4}{3}\pi R_G^3} = \frac{(1-\Phi)u_D}{u_D + u_C} \cdot \frac{1}{1 + 3\phi d_e / 2d_G} \tag{8}$$

where $\Phi$ and $d_e$ are the gas volume fraction and the equivalent diameter (0.8 mm in the microreactor), respectively. The enhancement of the mixing performance was mainly reflected in the form of modified flow rates, and the ratio between the bubble size and equivalent diameter of the pipe. To verify the accuracy of the modified dimensionless micromixing scale, $X_S$ and the corresponding $L^*$ were calculated at different operating conditions, as shown in Fig. 8b. Compared with the results of the homogeneous system, the dimensionless micromixing scale was apparently reduced by the introduction of microbubbles. The results demonstrated that the modified dimensionless micromixing scale was relatively precise. Furthermore, the mixing processes of the aqueous solution-based systems were similar. No other phase was introduced.

Based on the modified dimensionless micromixing scale $L^*$, the novel method of $BaSO_4$ nanoparticle preparation proposed in this paper was modeled. In our previous work, a proposed model was used to calculate the precipitation of $BaSO_4$ nanoparticles [26]. Combining the modified $L^*$and the precipitation model of $BaSO_4$ nanoparticles, the density distribution of the number of particles under smaller mixing scales was calculated, as shown in Fig. 9. The calculation was based on the classic precipitation theory and the population balance model as well as the presented parameters. The evolution of the particle number density can be clearly observed in every stage, as shown in Fig. 9. The total number of particles increased rapidly in the nucleation stage. With the microbubbles, $L^*$ could be reduced to 0.0016, which was almost 90%

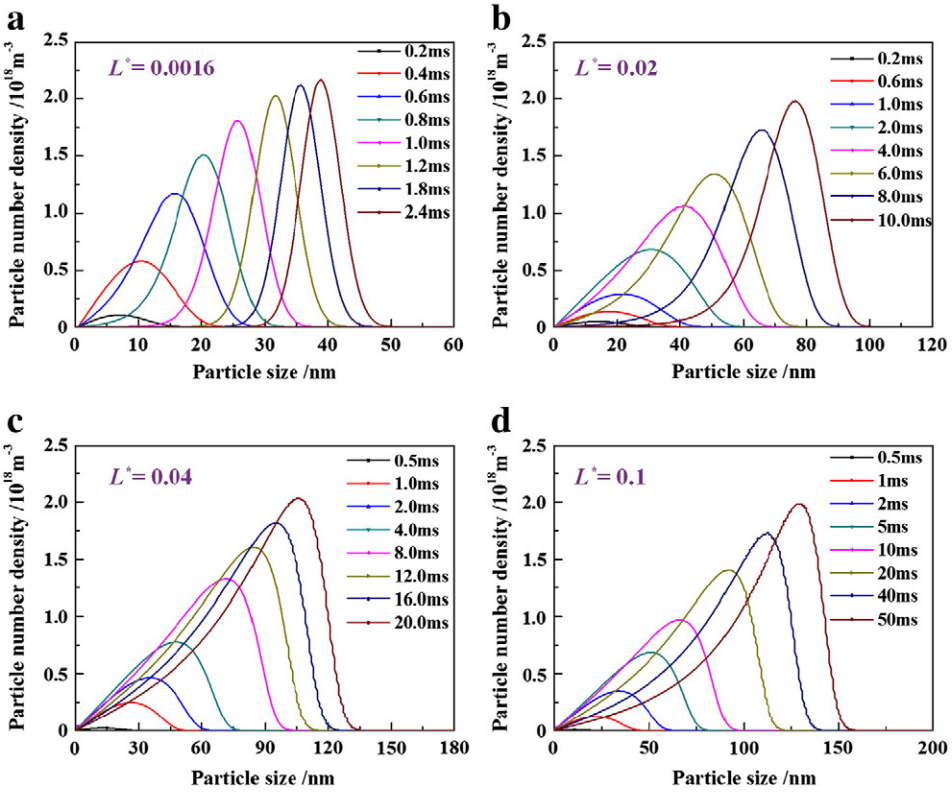


**Fig. 9.** Particle number density distribution under different mixing scales, BaS 2.12 mol·L$^{-1}$, $Na_2SO_4$ 0.32 mol·L$^{-1}$.

less than that of traditional L–L heterogeneous mixing. Most of the raw material was consumed in the nucleation stage, which caused few particles to grow after the efficient mixing. The reaction time in the precipitation process was similarly reduced by the enhanced mixing performance.

The distribution density function can be calculated from the density distribution of the number of particles. The comparison of the calculated results with the experimental data is presented in Fig. 10a to d. The calculated results were relatively consistent with the experiments. The influence of the gas flow rate and the reactant concentration on the mean particle size are illustrated in Fig. 10e and f, respectively, where the calculated results were consistent with the experimental data. Efficient mixing could adequately utilize the large supersaturation ratio, which caused the explosive nucleation and produced much smaller particles. The trends of the particle size variation were similarly consistent with the experimental results. Thus, the model could reasonably describe the $BaSO_4$ precipitation process of the microbubble system. However, this model still requires further research because of several assumptions that were made, such as the influence of the chemical reaction and mass transfer on the mixing scale.

## 4. Conclusions

Efficient mixing performance was achieved by introducing microbubbles into the working system with the membrane dispersion microreactor for nanoparticle synthesis. Consequently, high-quality $BaSO_4$ nanoparticles were successfully prepared at high reactant concentrations. The effects of the operating conditions on the mixing performance and particle size were investigated. The dispersed bubble size could be reduced to approximately 40 μm to 60 μm using high gas volume fraction. The mixing performance could be enhanced by continuously increasing the gas flow rate, despite bubble coalescence. The $BaSO_4$ nanoparticles were controllably prepared, with an average size of 40 nm. By contrast, only a minimum size of 1 μm was achieved in the barite industrial process. A dimensionless micromixing scale of the microbubbly flow was defined, and a model for the $BaSO_4$ precipitation process was proposed to predict the $BaSO_4$ particle size. The model was confirmed to be consistent with the experimental data. Therefore, the proposed process with its rapid microreaction could be easily scaled up, with great potential for its large-scale application.

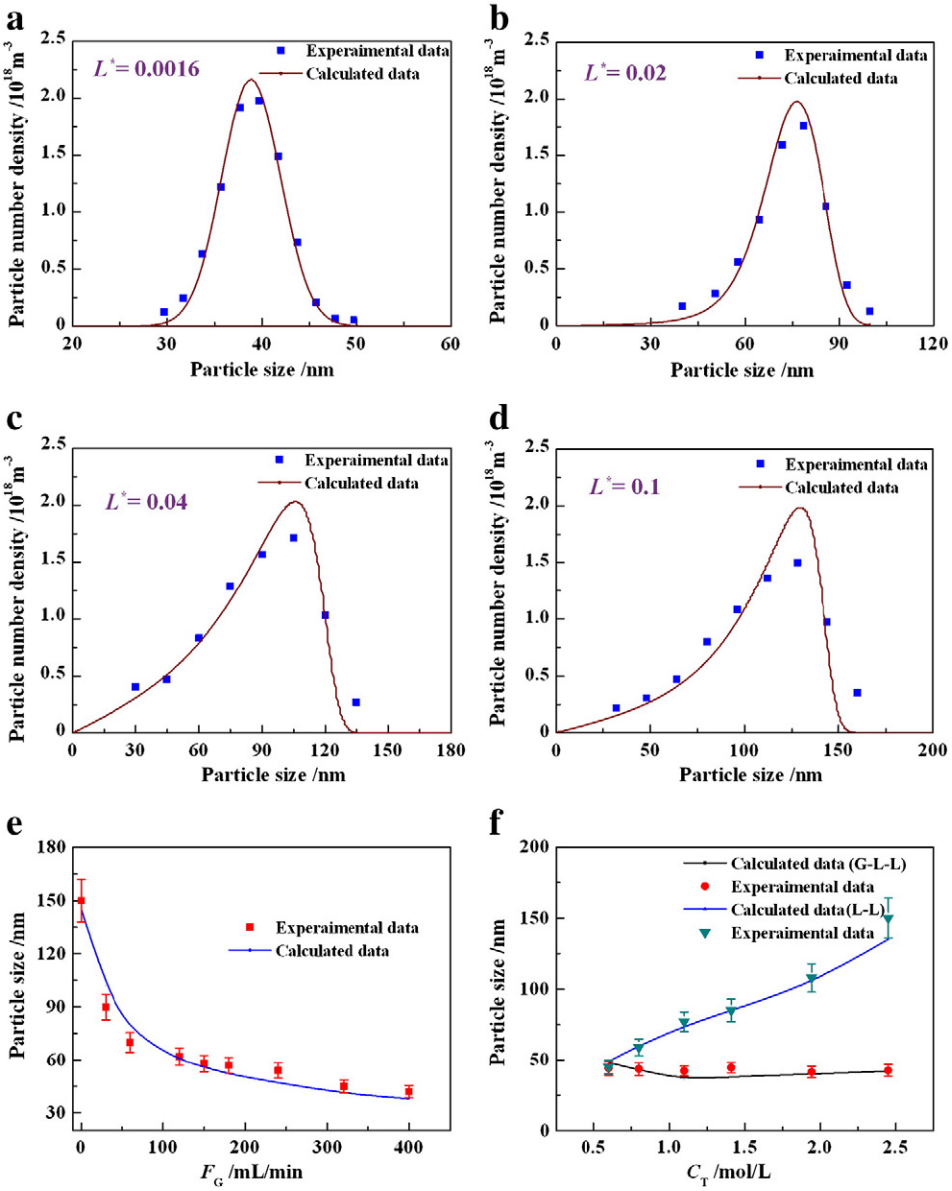


**Fig. 10.** The comparison of calculated distribution density function and average particle size with experimental results: (a–e) BaS 2.12 mol·L$^{-1}$, $Na_2SO_4$ 0.32 mol·L$^{-1}$; (f) $F_G$ = 150 mL·min$^{-1}$, $F_C$ = 120 mL·min$^{-1}$, $F_D$ = 48 mL·min$^{-1}$.

*Notation*

| | |
|---|---|
| $c_C$ | mole concentration of continuous feed, $mol \cdot L^{-1}$ |
| $c_D$ | mole concentration of dispersed feed, $mol \cdot L^{-1}$ |
| $d_{32}$ | Sauter mean particle diameter, nm |
| $d_G$ | diameter of microbubbles, μm |
| $d_e$ | equivalent diameter of the microreactor, mm |
| $F_C$ | flow rate of continuous feed, $mL \cdot min^{-1}$ |
| $F_D$ | flow rate of dispersed feed, $mL \cdot min^{-1}$ |
| $F_G$ | flow rate of $N_2$ gas, $mL \cdot min^{-1}$ |
| $L^*$ | dimensionless micromixing scale |
| $u_C$ | flow velocity of continuous feed, $m \cdot s^{-1}$ |
| $u_D$ | flow velocity of dispersed feed, $m \cdot s^{-1}$ |
| $u_G$ | flow velocity of $N_2$ gas, $m \cdot s^{-1}$ |
| $X_S$ | the segregation index |
| $\Phi$ | gas volume fraction, % |

## Acknowledgment

We gratefully acknowledge the supports of the National Natural Science Foundation of China (21036002) and National Basic Research Program of China (2012CBA01203) on this work.

## References

[1] H.J. Leng, X. Wang, G.L. Niebur, R.K. Roeder, Synthesis of a barium sulfate nanoparticle contrast agent for micro-computed tomography of bone microstructure, Ceramic Nanomaterials and Nanotechnology Iii 159 (2005) 219–229.
[2] H.C. Schwarzer, W. Peukert, Tailoring particle size through nanoparticle precipitation, Chemical Engineering Communications 191 (2004) 580–606.
[3] A. Petrova, W. Hintz, J. Tomas, Investigation of the precipitation of barium sulfate nanoparticles, Chemical Engineering and Technology 31 (2008) 604–608.
[4] J. Mulopo, J.N. Zvimba, H. Swanepoel, L.T. Bologo, J. Maree, Regeneration of barium carbonate from barium sulphide in a pilot-scale bubbling column reactor and utilization for acid mine drainage, Water Science and Technology 65 (2012) 324–331.
[5] H.G. Emblem, K. Hargreaves, Preparation, properties and uses of barium compounds, Reviews in Inorganic Chemistry 15 (1995) 109–137.
[6] G.H. Wu, Y.J. Wang, S.L. Zhu, J.D. Wang, Preparation of ultrafine calcium carbonate particles with micropore dispersion method, Powder Technology 172 (2007) 82–88.
[7] Y.J. Jung, S.H. Park, K.H. Song, J. Choe, Recrystallization of polyethylene submicron particles using a continuous flow micromixer system, Powder Technology 217 (2012) 325–329.
[8] R.M. Ribeiro-Costa, M.R. da Cunha, M.R. Gongora-Rubio, P. Michaluart-Junior, M.I. Re, Preparation of protein-loaded-PLGA microspheres by an emulsion/solvent evaporation process employing LTCC micromixers, Powder Technology 190 (2009) 107–111.
[9] S. Hasebe, Design and operation of micro-chemical plants — bridging the gap between nano, micro and macro technologies, Computers and Chemical Engineering 29 (2004) 57–64.
[10] Y. Song, J. Hormes, C.S.S.R. Kumar, Microfluidic synthesis of nanomaterials, Small 4 (2008) 698–711.
[11] H.C. Schwarzer, W. Peukert, Combined experimental/numerical study on the precipitation of nanoparticles, AICHE Journal 50 (2004) 3234–3247.
[12] Y. Ying, G.W. Chen, Y.C. Zhao, S.L. Li, Q. Yuan, A high throughput methodology for continuous preparation of monodispersed nanocrystals in microfluidic reactors, Chemical Engineering Journal 135 (2008) 209–215.
[13] J. Cheng, C. Yang, Z.-S. Mao, C. Zhao, CFD modeling of nucleation, growth, aggregation, and breakage in continuous precipitation of barium sulfate in a stirred tank, Industrial and Engineering Chemistry Research 48 (2009) 6992–7003.
[14] H.Y. Wei, W. Zhou, J. Garside, Computational fluid dynamics modeling of the precipitation process in a semibatch crystallizer, Industrial and Engineering Chemistry Research 40 (2001) 5255–5261.
[15] J.M. Rousseaux, C. Vial, H. Muhr, E. Plasari, CFD simulation of precipitation in the sliding-surface mixing device, Chemical Engineering Science 56 (2001) 1677–1685.
[16] J. Baldyga, W. Podgorska, R. Pohorecki, Mixing-precipitation model with application to double feed semibatch precipitation, Chemical Engineering Science 50 (1995) 1281–1300.
[17] T. Sakai, K. Sawada, N. Ohi, A kinetic-study of liquid-phase oxidation of sodium sulfide with oxygen catalyzed by sulfur black-B dye, Journal of Chemical Engineering of Japan 13 (1980) 331–334.
[18] D. Ahmed, X. Mao, B.K. Juluri, T.J. Huang, A fast microfluidic mixer based on acoustically driven sidewall-trapped microbubbles, Microfluidics and Nanofluidics 7 (2009) 727–731.
[19] Y.L. Ding, Z.L. Wang, M. Ghadiri, D.S. Wen, Vertical upward flow of gas–solid two-phase mixtures through monolith channels, Powder Technology 153 (2005) 51–58.
[20] X. Mao, B.K. Juluri, M.I. Lapsley, Z.S. Stratton, T.J. Huang, Milliseconds microfluidic chaotic bubble mixer, Microfluidics and Nanofluidics 8 (2010) 139–144.
[21] A.D. Stroock, S.K.W. Dertinger, A. Ajdari, I. Mezic, H.A. Stone, G.M. Whitesides, Chaotic mixer for microchannels, Science 295 (2002) 647–651.
[22] G.G. Chen, G.S. Luo, S.W. Li, J.H. Xu, J.D. Wang, Experimental approaches for understanding mixing performance of a minireactor, AICHE Journal 51 (2005) 2923–2929.
[23] K. Wang, Y.J. Wang, G.G. Chen, G.S. Luo, J.D. Wang, Enhancement of mixing and mass transfer performance with a microstructure minireactor for controllable preparation of $CaCO_3$ nanoparticles, Industrial and Engineering Chemistry Research 46 (2007) 6092–6098.
[24] L. Du, J. Tan, K. Wang, Y.C. Lu, G.S. Luo, Controllable preparation of $SiO_2$ nanoparticles using a microfiltration membrane dispersion microreactor, Industrial and Engineering Chemistry Research 50 (2011) 8536–8541.
[25] S.W. Li, J.H. Xu, Y.J. Wang, G.S. Luo, Mesomixing scale controlling and its effect on micromixing performance, Chemical Engineering Science 62 (2007) 3620–3626.
[26] S.W. Li, J.H. Xu, Y.J. Wang, G.S. Luo, Modeling of nano-particle precipitation process in a membrane dispersion micro-structured reactor, Powder Technology 195 (2009) 213–220.
[27] M.C. Fournier, L. Falk, J. Villermaux, A new parallel competing reaction system for assessing micromixing efficiency — experimental approach, Chemical Engineering Science 51 (1996) 5053–5064.
[28] G.G. Chen, G.S. Luo, Y. Sun, J.H. Xu, J.D. Wang, A ceramic microfiltration tube membrane dispersion extractor, AICHE Journal 50 (2004) 382–387.
[29] G.S. Luo, L. Du, Y.J. Wang, Y.C. Lu, J.H. Xu, Controllable preparation of particles with microfluidics, Particuology 9 (2011) 545–558.
[30] D. Jeevarathinam, A.K. Gupta, B. Pitchumani, R. Mohan, Effect of gas and liquid flowrates on the size distribution of barium sulfate nanoparticles precipitated in a two phase flow capillary microreactor, Chemical Engineering Journal 173 (2011) 607–611.
[31] C.B.B. Costa, R.M. Filho, Nanoparticle processes modelling: the role of key parameters for population balances for on-line crystallization processes applications, Powder Technology 202 (2010) 89–94.
[32] J.-P. Guillemin, E. Schaer, P. Marchal, C. Lemaitre, H. Nonnet, A. Ledieu, A mass conservative approach to model the ultrasonic de-agglomeration of ZnO nanoparticle suspension in water, Powder Technology 219 (2012) 59–64.
[33] B. Niemann, K. Sundmacher, Nanoparticle precipitation in microemulsions: population balance model and identification of bivariate droplet exchange kernel, Journal of Colloid and Interface Science 342 (2010) 361–371.